Journal of Alloys and Compounds 750 (2018) 304–311

Contents lists available at ScienceDirect

Journal of Alloys and Compounds

journal homepage: http://www.elsevier.com/locate/jalcom

# $Ho^{3+}$-$Yb^{3+}$:$YMoO_4$ core@shell nanoparticles for enhanced visible upconversion and security applications

Manisha Mondal, Vineet Kumar Rai*

*Laser and Spectroscopy Laboratory, Department of Applied Physics, Indian Institute of Technology (Indian School of Mines), Dhanbad, 826004, Jharkhand, India*

ARTICLE INFO

*Article history:*
Received 15 November 2017
Received in revised form
10 March 2018
Accepted 12 March 2018
Available online 13 March 2018

*Keywords:*
Core@shell
Nanoparticles
TEM
Upconversion
Security ink

ABSTRACT

$Ho^{3+}$-$Yb^{3+}$ sensitized $YMoO_4$ core@shell upconversion (UC) nanoparticles (NPs) have been structurally and optically characterized. Bright Field Transmission Electron Microscopy (TEM) imaging and the corresponding Fast Fourier Transform (FFT) pattern has been done to evidence the formation of core@shell nanostructures. Optical properties viz. UV–Vis absorbance spectra, Dynamic Light Scattering (DLS), zeta potential measurement and upconversion (UC)/downconversion (DC) spectra of core and core@shell nanoparticles have been reported. The core@shell NPs exhibits both the colloidal stability and solubility in well suited biological liquids. Due to silica shell across the $Ho^{3+}$/$Yb^{3+}$ codoped $YMoO_4$ NPs, the frequency UC emission intensity of all bands have been increased compared to that of core NPs. The colour emitted from the core@shell NPs lies in the green region having colour purity ~95%. In biocompatible solvents under 980 nm excitation, the reduction in the overheating problem is due to small decrement in the UC emission intensity of core@shell NPs compared to that of the core NPs.



## 1. Introduction

Rare earths (REs) doped upconversion (UC) nanoparticles (NPs) have attracted significant interest because of their applications in the field of UC lasers, IR quantum counters, solid state lighting devices, security levels, LEDs, biological imaging, biosensing, photodynamic therapy (PDT), etc. [1–9]. Many obstacles have been found in the applications of UC NPs because of their poor water solubility due to the presence of hydrophobic organic ligands on the surface. This causes the negative influence to biological tissues [10]. Due to low solubility in water and incompatible surface property of the UC NPs, they cannot be used for biological applications. However, the core@shell nanomaterials and nanostructures have become an important research area due to their applications in different fields. Optical properties of the core@shell nanomaterials will be different from its core nanomaterials and depending on different surface morphologies of core and shell with varying thickness, their functional properties can be tuned [11–14]. Shao et al. studied the upconversion luminescence, temperature sensing and photothermal conversion properties in the lanthanides doped core/shell nanoparticles under 980/808 nm excitation. They reported that the developed nanoparticles can be used in imaging-guided and temperature-monitored photothermal treatments [14]. The biodegradable silica rubber core-shell nanoparticles and their stereocomplex for poly lactic acid (PLA) advanced composites applications have been reported by Li et al. [15]. Till now, various core@shell nanoparticles have been successfully developed to produce hydrophilic and biocompatible UC NPs [15–18]. To improve the UC luminescence efficiency, researchers are trying to grow shell of inert inorganic materials around the rare earth ions doped core materials. The enhancement in luminescence efficiency occurs due to the sufficient energy transfer from sensitizer to the activator ions and also the shell can shield the dopant ions and inhibits the defect sites on the particles surface from luminescence quenching. But due to the hydrophobic nature and poor biological conjugation activity, some of the inorganic shell materials cannot be used in the biological fields [19,20]. Among the various surface coating processes, silica coating formation is very simple and good technique because of its high specific surface area, optical transparency, chemical inertness, excellent biocompatibility, high photochemical stability, nontoxicity and further concomitance with other functional groups [21–23].

Due to the excellent thermal stability and luminescent properties, rare earths doped molybdate materials have been studied in

* Corresponding author.
*E-mail addresses:* vineetkrrai@yahoo.co.in, vineetkrrai@iitism.ac.in (V.K. Rai).

https://doi.org/10.1016/j.jallcom.2018.03.148
0925-8388/

various fields such as phosphors, laser hosts, upconversion, biolabeling, etc. [24]. Among $AMoO_4$ materials, the $YMoO_4$ host having scheelite type tetragonal structure due to the luminescent $MoO_4$ tetrahedron cluster unit, serves as an excellent host material in the luminescent fields [25,26]. On the other hand, triply ionized holmium ions are very good activator due to their various energy levels to reach visible UC emission. The UC luminescence intensity can be enhanced by codoping with suitable sensitizers. The frequency UC luminescence intensity can also be improved by developing the shell around the core NPs. Triply ionized ytterbium ions are suitable sensitizer under 980 nm NIR diode laser excitation, because it has large absorption cross-section at 980 nm. The $YMoO_4$ has been taken as a host material for the $Ho^{3+}$ ions because the ionic radius of $Ho^{3+}$ ions (104.1 p.m.) is similar to the $Y^{3+}$ ions (104 p.m.) [27,28]. Due to similar ionic radii, $Ho^{3+}$ ions may occupy the $Y^{3+}$ sites keeping sharp emission bands. On codoping with the $Li^{+}$ ions in the $Ho^{3+}/Yb^{3+}$:$YMoO_4$ NPs, an enhancement of about ~2 times in the green emission band has been reported [29].

Based on the different synthesis procedures using silica as shell material, a variety of core@shell structured materials have been prepared. For example, $Fe_3O_4$@$SiO_2$, $Gd_2O_3$:$Eu^{3+}$@$SiO_2$, BaFBr-$Eu^{2+}$@$SiO_2$ were obtained by different strategic routes such as reverse microemulsion method, sol-gel method, Stöber method, etc. [30–32]. Stöber method is much simpler and easy process that has possibility to transfer the NPs into aqueous solvents. To the best of our knowledge, the silica surface modified $Ho^{3+}/Yb^{3+}$:$YMoO_4$ core NPs synthesized via Stöber method have not been prepared and the frequency upconversion emission properties under 980 nm diode laser excitation used for the present study have not been reported till date.

## 2. Experimental section

### 2.1. Chemicals

Yttrium oxide ($Y_2O_3$), ammonium hepta molybdate ($[NH_4]_6Mo_7O_{24}$*$4H_2O$), holmium oxide ($Ho_2O_3$), ytterbium oxide ($Yb_2O_3$), aqueous ammonia, tetraethyl orthosilicate (TEOS) and ethanol were used as received without further purification. The distilled water used was purified by a Millipore system.

### 2.2. Synthesis

#### 2.2.1. Synthesis of $Ho^{3+}$-$Yb^{3+}$:$YMoO_4$ core nanoparticles (NPs)

The analytical grade (AR) yttrium oxide ($Y_2O_3$, 99.999%, Central Drug House, India), ammonium heptamolybdate tetrahydrate [$(NH_4)_6Mo_7O_{24}\cdot 4H_2O$, E- Merck, India], ytterbium oxide ($Yb_2O_3$, 99.9%, Central Drug House, India), holmium oxide ($Ho_2O_3$, 99.99%, Central Drug House, India), ethanol (99.9%, Analytical reagent) were used as starting materials to prepare the $Ho^{3+}$-$Yb^{3+}$:$YMoO_4$ nanophosphors [29].

At first, the oxide materials were mixed with nitric acid ($HNO_3$) to form their nitrates. After formation of yttrium nitrate, it was dissolved into ammonium hepta molybdate to form yttrium molybdate [29]. For preparing the $Ho^{3+}$-$Yb^{3+}$:$YMoO_4$ nanophosphors the concentration of the $Ho^{3+}$ ions were taken as 0.3, 0.5 and 0.7 mol% whereas the concentration of the $Yb^{3+}$ ions were taken as 2.0, 4.0, 5.0, 7.0 mol%. The dopants $Ho^{3+}$, $Yb^{3+}$ were mixed with the host material in the form of their nitrates and the solution was then heated at 70 °C. The ammonia solution was added to the transparent solution to get the precipitate and then it was kept for 24 h at room temperature. The precipitate was then filtered and washed three times with deionized water and ethanol. The obtained precursor was kept in an electric furnace for 15 min at 550 °C to get the powder form. Further, the phosphors were kept for 2 h at 800 °C for annealing to improve crystallinity.

#### 2.2.2. Coating of $Ho^{3+}$-$Yb^{3+}$:$YMoO_4$ nanoparicles with $SiO_2$ shell

The core@shell NPs have been prepared by Stöber method [33]. The synthesized core NPs (50.0 mg) were well dispersed in a mixed solution of deionized water (50.0 ml), ethanol (70.0 ml) and concentrated aqueous ammonia solution (1.0 ml) in a three neck round bottom flask. Afterward, 1.0 ml TEOS was added in 2.0 min and the reaction was allowed to proceed for 6.0 h under continuous stirring at room temperature. After 6.0 h of continuous mechanical stirring at room temperature, the silica coated core@shell NPs were separated by centrifugation. The prepared core@shell NPs were then washed with ethanol and dried at room temperature.

### 2.3. Material characterization

For X-ray Diffraction (XRD) measurements, the prepared samples were kept in a smooth surface sample holder at an angle of 45°. A Bruker D8 advanced X-ray diffractometer with CuKα radiation (k = 1.54 Å) has been used for the XRD study of the prepared NPs. For Transmission Electron Microscopy (TEM) imaging, High Resolution TEM (HRTEM) imaging and Energy Dispersive X-ray Spectroscopy (EDS) analysis, a FEI Tecnai F30 transmission electron microscope (TEM) operating at 300 keV was used. The optical absorption spectra have been performed by using the UV–Vis–NIR spectrophotometer (Model no- Agilent Cary 5000). The frequency UC emission has been performed with a Princeton triple turret grating monochromator connected with a photomultiplier tube (PMT) upon excitation with a continuous wave (CW) laser diode lasing at 980 nm. All the measurements were performed at room temperature.

## 3. Results and discussion

### 3.1. Formation and morphology of core@shell nanoparicles

The phase compositions of the prepared core and core@shell NPs have been identified with the help of the X-ray diffraction (XRD) studies. The X-ray diffraction patterns of the core and core@shell NPs are shown in Fig. 1 (a). The XRD patterns of all the samples are matching very well with JCPDS file no. 35-1470. The lattice constants are $a = b = 5.168$ Å, $c = 11.002$ Å and $\alpha = \beta = \gamma = 90°$. The diffraction peaks of the prepared $Ho^{3+}$-$Yb^{3+}$ codoped core@shell NPs are found at diffraction angles (2θ) at 29.46, 32.91, 34.45, 48.40, 49.55, 56.23, 58.26 and 60.83 corresponding to (112), (004), (200), (204), (220), (116), (312) and (224) planes respectively [29]. The diffraction peaks positions of the core and core@shell NPs are matching well which implies that the $Ho^{3+}$-$Yb^{3+}$:$YMoO_4$ NPs are not influenced by $SiO_2$ shell. Both the samples have the tetragonal phase with space group $I41/a$ (88) of $YMoO_4$. The average crystallite size of the prepared core and core@shell NPs has been calculated by Debye-Scherrer's formula [34–37]. The crystallite size of the developed core and core@shell NPs are found to be ~35 nm and ~38 nm respectively. The broad peaks observed in Fig. 1 (a) are due to the nanocrystalline nature of the prepared samples.

Bright field Transmission Electron Microscopy (TEM) images confirm the formation of the core@shell NPs across the core material. It is observed from Fig. 1 (b) that the as prepared cores NPs have well defined size distribution of average particle size ~ 47 nm. Fig. 1 (c) shows that the obtained silica coated core@shell NPs still retain the uniform morphology. Bright field TEM images confirm that the layer of coating has an average shell thickness of ~5 nm. No significant change in the morphology and composition of silica coated core NPs after the surface modification by $SiO_2$ was

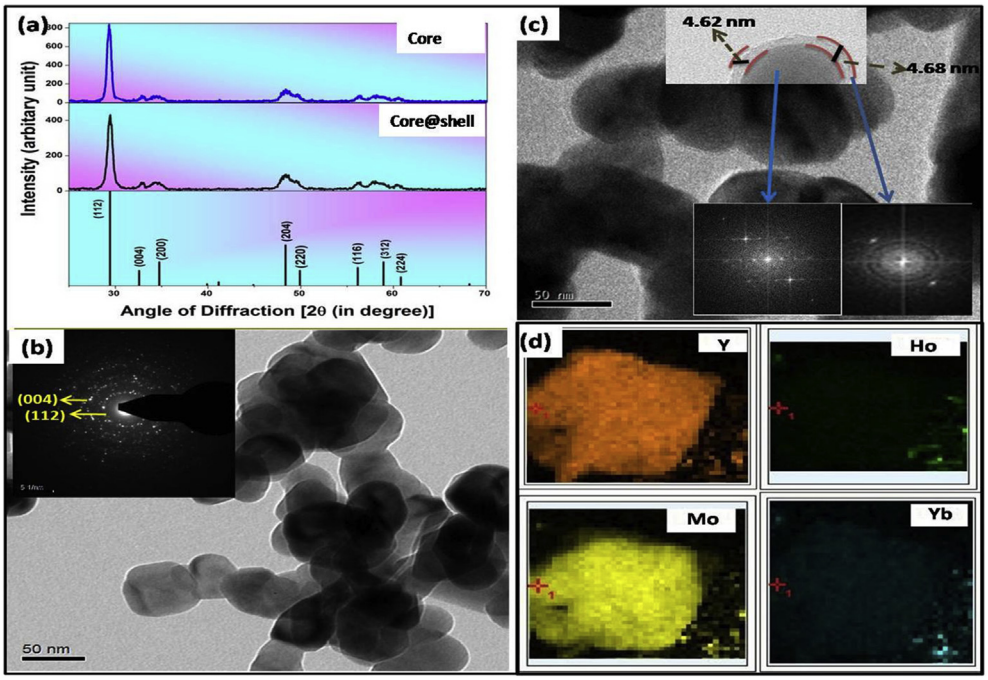


**Fig. 1.** (a) X-ray Diffraction patterns of the core and core@shell nanoparticles, Bright field TEM images of (b) core nanoparticles (inset shows the SAED pattern), (c) core@shell nanoparticles (inset shows the zoom view of the core@shell NPs and the corresponding FFT pattern) (d) The EDS mapping across a particle in the core@shell NPs.

observed. The Selected Area Electron Diffraction (SAED) pattern {inset of Fig. 1 (b)} shows the spotty ring patterns of the prepared samples thereby indicating the polycrystalline nature of the developed NPs. The rings corresponding to the {(112), (004)} planes of the $YMoO_4$ NPs are in consistent with the XRD results. To investigate the core@shell structure more clearly in the core@shell NPs, FFT patterns {shown in inset of Fig. 1 (c)} of the crystalline grains and boundaries are obtained. In the FFT patterns, the grain and boundaries show the clear spot and diffuse ring patterns respectively, thereby confirming the presence of the silica shell [38]. The representative compositional mapping of the NPs has been done to know the distribution of the individual elements {Fig. 1 (d)}.

### 3.2. Optical properties

UV–Visible absorption spectra of the $Ho^{3+}$-$Yb^{3+}$:$YMoO_4$ core and silica surface modified core NPs dispersed in distilled water with the help of ultrasonic bath were recorded at room temperature within the range 1.55–6.2 eV. The deviation in absorbance at longer wavelength observed for the core and core@shell NPs is due to the different scattering behavior of the solvents [25]. A broad absorption band within 4.13–6.20 eV is attributed to the charge transfer from the oxygen (2p) shells to $Mo^{5+}$ ions inside the $MoO_4$ groups [39]. The absorption spectra of the developed NPs show almost similar features but the edge of the absorption bands are different. This difference in the band edge occurs due to the formation of thinner silica layer around the core NPs. From the Fig. 2 (a) one can see that the band edge in silica coated $Ho^{3+}$-$Yb^{3+}$:$YMoO_4$ NPs shifts towards the lower potential side. The high absorbance of the core NPs is due to the charge transfer (CT) mechanism inside the molybdate groups. The shift in the absorption band is because of the interaction between molybdate groups and coating layer, which causes the change in coordination geometry and hence the symmetry of materials [40]. An additional advantage of the $SiO_2$ coating in NPs is that, it allows the hydrogen bonding with protic glacial solvents such as water and methanol as well as Vander Walls' weak interactions with aprotic polar solvents such as DMSO (Dimethyl Sulfoxide). The colloidal stability of the core@shell NPs has been tested by dissolving 10 mg of the material in 10 ml of water, methanol and DMSO, respectively, with the help of an ultrasonic bath and their sedimentation was observed after 1 day and 1 week. The sedimentation of the core@shell NPs dispersed in water is shown in Fig. 2 (b). The resultant silica surface modified core@shell NPs exhibit better dispersibility as well as colloidal stability in water, methanol and DMSO than that of the core NPs after 24 h. Due to the excellent colloidal stability and dispersibility the core@shell NPs can be used for biological applications. The silica coated core NPs can be used for drug delivery, fluorescence imaging and also in different bio-related applications. Because of its smaller size, it can escape from phagocytes in the reticuloendothelial (RES) system, such as spleen and liver, and circulate through blood vessels with a long blood half life but the larger NPs cause rapid uptake by the RES system [33,41]. No clear agglomeration with the naked eyes was noted after keeping the NPs for two weeks. The presence of silica layer not only shows high dispersibility in water, it also allows conjugation with various bio-molecules due to the presence of silanol molecules. Moreover, the band gap energy of the prepared core and core@shell NPs in its powder have been determined by the Tauc relation [42] and the energy band gap is found to be ~2.99 and ~2.96 eV for the core and core@shell NPs respectively {Electronic Supplementary Material (ESM) Fig. 1 (a)}. The reduction in the band gap occurs due to the fitting errors.

Moreover, to confirm the colloidal stability of the NPs in water Dynamic Light Scattering (DLS) and the corresponding zeta potential measurements have been carried out. The hydrodynamic diameter of the core@shell NPs have been found to be about ~110 nm in neutral water (pH~ 7) and showed negligible change after one week {ESM Fig. 1 (b)}. The zeta potential of the core@shell NPs is about ~26 mV thereby indicating the good stability of the NPs.

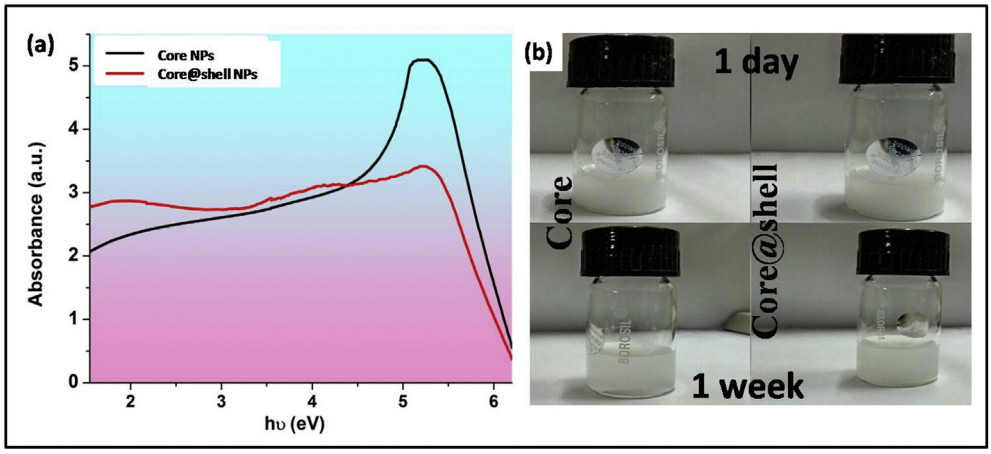


**Fig. 2.** (a) UV–Vis absorption spectra, (b) Photograph taken after dispersing core and core@shell nanoparticles in water.

*3.2.1. Photoluminescence study*

The host materials containing $VO_4$, $NbO_4$, $WO_4$, and $MoO_4$ groups, commonly known as self activated phosphors, are very important now a day's for various photonic applications. The downshifting photoluminescence (PL) behavior of the core and core@shell NPs have been studied under 293 nm UV excitation. The broad band observed in the large part of the visible electromagnetic spectrum attributes to multiphonon and multilevel process, i.e., relaxation occurs in a system via several paths involving the participation of numerous states within the band gap of the material. It is observed that under 293 nm UV excitation {ESM Fig. 2 (a)}, which falls in the broad absorption range of the molybdate host {Fig. 3 (a)}, the emission occurs due to charge transfer transitions from 4 d state of Mo (below the conduction band) to oxygen 2p states (near the valance band) in the $MoO_4$ group. The $MoO_4$ group in the host lattice is deexcited radiatively and produces broad emission within 400–650 nm region with maximum peak intensity around ~470 nm [43]. The f-f transitions in the $Ho^{3+}$ ions are relatively weak and it is hard to detect the emissions arising from the $Ho^{3+}$ ions. The emission intensity is noted maximum in the core@shell NPs, indicating that the coating of silica decreases the nonradiative relaxations via surface defects of NPs and hence causes an increase in the intensity.

The UC luminescence observation in the core and core@shell NPs excitated at 980 nm within 13.18–61.29 W/cm$^2$ excitation density has been performed. The UC emission spectra of $Ho^{3+}$

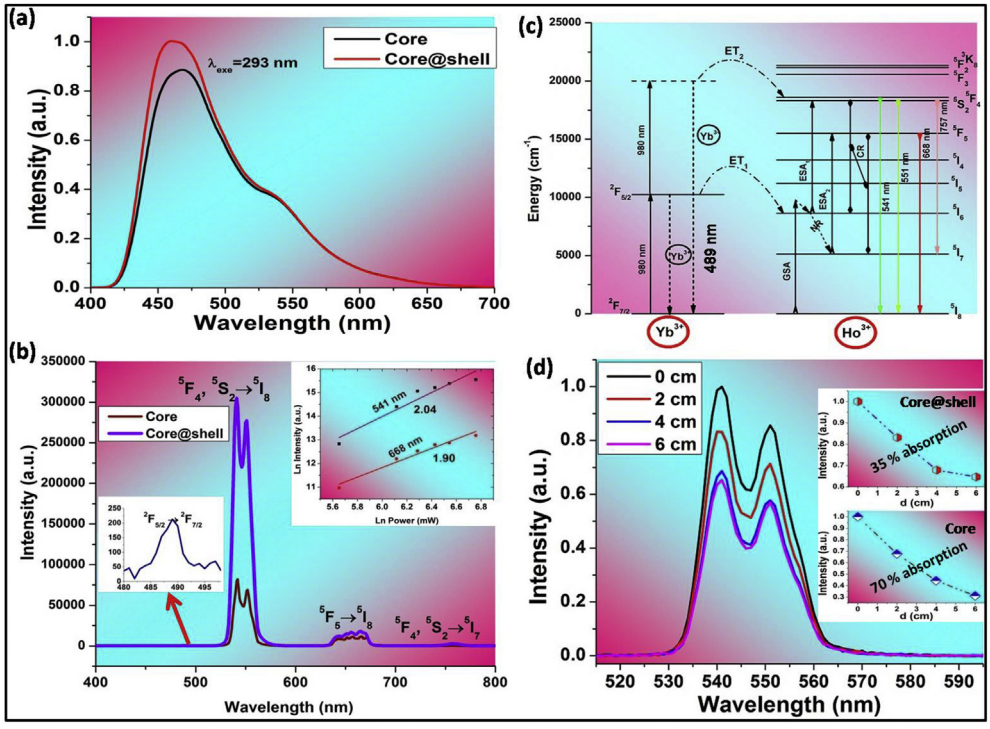


**Fig. 3.** (a) Downconversion emission spectra under 293 nm excitation of core and core@shell nanoparticles (b) Upconversion emission spectra under 980 nm excitation at 29.42 W/cm$^2$ pump power density, (c) Schematic representation of energy level diagram of the $Ho^{3+}$-$Yb^{3+}$ system with the possible transitions (d) Upconversion luminescence spectra under 980 nm excitation with different depths of water of the core@shell nanoparticles (inset shows the variation of 541 nm emission intensities with different depths of water for core and core@shell nanoparticles).

doped $YMoO_4$ NPs on varying the concentration of $Ho^{3+}$ ions from 0.3 to 0.7 mol% have been recorded [29]. The maximum UC emission intensity was observed at 0.5 mol% $Ho^{3+}$ ions concentration and above this value the UC emission intensity decreases due to concentration quenching. Taking the optimum concentration of the $Ho^{3+}$ ions, the concentration of $Yb^{3+}$ ions is varied from 1.0 to 5.0 mol% to prepare the $Ho^{3+}$-$Yb^{3+}$ codoped $YMoO_4$ NPs. The UC emission intensity increases with increasing the $Yb^{3+}$ ions concentration and the maximum UC emission intensity is reported at 0.5 mol% $Ho^{3+}$+4.0 mol% $Yb^{3+}$ combination. Further, on increasing the $Yb^{3+}$ ions concentration (>4.0 mol%) the UC emission intensity decreases [29].

A comparative spectral investigation of the optimized core and core@shell NPs carried out upon 980 nm NIR CW diode laser excitation at room temperature is shown in Fig. 3 (b). The optimized 0.5 mol% $Ho^{3+}$-4.0 mol% $Yb^{3+}$: $YMoO_4$ core NPs shows three emission bands peaking at 541 nm, 551 nm and 668 nm in the green and red regions corresponding to the $^5F_4$, $^5S_2$ → $^5I_8$ and $^5F_5$ → $^5I_8$ electronic transitions, respectively. The UC emission bands lying in the green and red regions have been significantly increased in the codoped core NPs compared to that of the $Ho^{3+}$ singly doped $YMoO_4$ core NPs due to the efficient energy transfer from $Yb^{3+}$ to the $Ho^{3+}$ ions [29,44,45]. The UC emission intensity of all the bands have been further increased on developing the silica layer around the $Ho^{3+}$-$Yb^{3+}$ codoped $YMoO_4$ core NPs. The enhancement of about ~5 times for the green band and ~2 times for the red band has been reported {Fig. 3 (b)}. One extra band at 757 nm corresponding to the $^5F_4$, $^5S_2$ → $^5I_7$ transition was also observed in the core@shell NPs. UC emission intensity enhancement becomes ~250 times for the green band in the $Ho^{3+}$-$Yb^{3+}$ codoped $YMoO_4$ core@shell NPs as compared to that of the $Ho^{3+}$ singly doped $YMoO_4$ core NPs. The spectral profile shows that both the core and core@shell NPs exhibit similar transitions except their intensity changes, which further confirms the identical environment of the core and core@shell NPs.

Interestingly, the enhancement in UC emission intensity occurs after shelling the core with silica layer. As the silica itself does not show crystalline nature as well as UC luminescence, but the silica coated NPs show higher UC emission intensity for the green and red bands. The enhancement in UC intensity occurs due to reduction in the surface defect density on the core@shell NPs due to presence of silica coating [46]. On increasing the pump power density the UC emission intensity is increased. The enhancement observed in UC emission intensity in the core@shell NPs is attributed due to the shell shielding effect over the core from quenching arising from ligands and solvents (i.e., surfactant hydroxyl groups) in the surface of UC NPs [47–50].

The involvement of number of NIR pump photons in the UC process can be obtained from the pump power dependence study of various emission bands by using the following relation [51],

$$I_{up} \propto P_{up}^{n}$$

where, "$I_{up}$" represents the intensity of UC emission band, "$P_{up}$" represents the pump power of the excitation source and "n" is the number of pump photons that are taking part in the UC process. Subsequently, the slope of logarithmic UC emission intensity versus logarithmic pump power shows the number of pump photons required in the UC process. The pump power dependence versus UC emission intensity study shows the involvement of two NIR photons {shown in inset of Fig. 3 (b)} for both the green (541 nm) and red (668 nm) bands [44,45]. Further, the increment in UC emission intensity for core@shell NPs than that of the core NPs was investigated in presence of coating of the silica layer that protects the dopants present near at the surface of core from quenching arising from surfactant hydroxyl groups. The UC mechanisms of the prepared core/core@shell NPs could be explained by considering the energy level diagram shown in Fig. 3 (c).

The mechanisms involved in the UC process are mainly the ground state absorption (GSA), excited state absorption (ESA) and energy transfer (ET). It is observed from energy level diagram that there is energy mismatch between the energy of 980 nm photons and the $^5I_6$ level of $Ho^{3+}$ ions. Whereas, the energy of the $^2F_{5/2}$ level of the $Yb^{3+}$ ions matches well with the 980 nm photons energy so that the $Yb^{3+}$ ions sufficiently absorb the 980 nm pump photons [29]. In case of the $Ho^{3+}$:$YMoO_4$ NPs, after absorbing 980 nm photons the $Ho^{3+}$ ions by ground state absorption (GSA) process jump to the $^5I_6$ level followed by the nonradiative relaxation process. Reabsorbing another 980 nm pump photons some of the triply ionized holmium ions from the $^5I_6$ level reaches to the $^5F_4$, $^5S_2$ level via $ESA_1$ process, from where it relaxes to the $^5I_8$ and $^5I_7$ levels emitting photons in the green and NIR region corresponding to the $^5F_4$, $^5S_2$→ $^5I_8$ and $^5F_4$, $^5S_2$→ $^5I_7$ transitions respectively. The rest of the $Ho^{3+}$ ions which are in the $^5I_6$ level relax nonradiatively to the $^5I_7$ level and then by $ESA_2$ process transit upward to the $^5F_5$ level. The excited $Ho^{3+}$ ions relax radiatively to the $^5I_8$ level by emitting red light (668 nm). However, the UC emission intensity of the $Ho^{3+}$-$Yb^{3+}$:$YMoO_4$ codoped core NPs is higher than that of the $Ho^{3+}$:$YMoO_4$ core NPs. This is basically due to the efficient energy transfer ($ET_1$ and $ET_2$) and cross-relaxation ($^5F_5$+$^5I_6$ ↔ $^5I_7$+$^5S_2$, $^5F_4$) along with the GSA, $ESA_1$, $ESA_2$ processes. The possible existence of the UC emission band at ~489 nm {inset in Fig. 3 (b)} corresponding to the $2^2F_{5/2}$ → $2^2F_{7/2}$ transition ($Yb^{3+}$) confirms the involvement of cooperative energy transfer process among the $Yb^{3+}$ ions in the $^2F_{5/2}$ state and hence also the energy transfer process ($ET_2$) from the $Yb^{3+}$ to $Ho^{3+}$ ions.

The core@shell NPs are more suitable in biological applications due to lower decrement in the UC emission intensity than the core NPs when these NPs are dissolved in different biocompatible solvents for detecting the interior under 980 nm laser diode excitation. The UC emission spectra of the green band in both core and core@shell NPs with different depths of biological solvents such as water, methanol and DMSO have been recorded. It has been observed that through 6.0 cm depth of water, the UC emission intensity was absorbed ~70% and ~35% in the core and core@shell NPs respectively {Fig. 3 (d)}. This indicates that the measured emission intensity of core@shell NPs is higher than that of the core NPs in different biocompatible solvents, because the shell is shielding the emitting ions from the quenching effect of surrounding solvents and reduces the surface defects density. Similar results have been analyzed in these three kinds of solvents. The UC emission intensity has been reduced significantly when the NPs were dissolved in DMSO due to its higher dipolar moment. According to the time dependent Schrodinger's equation, the absorption coefficient is directly proportional to the dipole moment [52,53]. The dipole moment of DMSO, methanol and water are ~3.6 D, ~1.65 D and ~1.86 D, respectively [54–56]. Higher dipole moment of DMSO induces higher absorption coefficient. The higher value of the absorption coefficient acts as a quenching source which inhibits the UC emission intensity.

The time-resolved fluorescence spectra were recorded using a single photon counting technique with a microsecond Xenon flash lamp as the source of excitation. The decay profile was monitored under 293 nm excitation for the green emission band of the $Ho^{3+}$ ions by microsecond xenon flash lamp {Fig. 4 (a) and (b)}. The calculated fluorescence decay time of the $^5F_4$, $^5S_2$ level is found to be $6.04 \pm 0.081$ μs for the core NPs, whereas it is $5.74 \pm 0.70$ μs for core@shell NPs. This implies that the transition probability of the emitting level in the core@shell NPs is relatively higher compared to that of core NPs. Such a reduction in decay time suggests that the surface modified silica core NPs results reduction in the surface

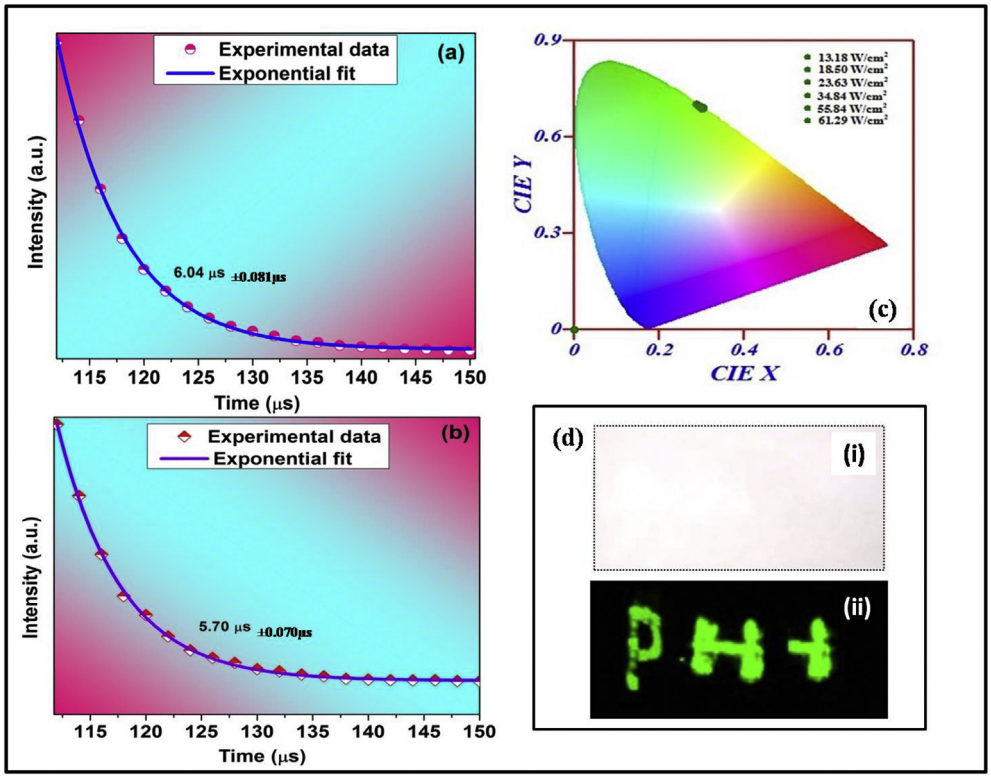


**Fig. 4.** Fluorescence decay curves for the $^5F_4$, $^5S_2 \rightarrow {}^5I_8$ green emission of $Ho^{3+}$ ions in (a) core (b) core@shell nanoparticles (c) Calculated CIE colour coordinates at different pump power densities (d) Photo taken (i) before and (ii) after 980 nm laser radiation, incident on written matter by using core@shell NPs at 34.84 W/cm$^2$ of pump power density. (For interpretation of the references to colour in this figure legend, the reader is referred to the Web version of this article.)

defects and it leads to a faster excitation of the emitting levels [51]. By reducing the surface defects via nonradiative recombination, the luminescence decay time decreases, and therefore the luminescence intensity increases in the core@shell NPs [57].

### 3.2.2. Photometric characterization and security ink applications

The chromaticity diagram of developed core@shell NPs at different pump power densities is shown in Fig. 4 (c). The colour emitted by the developed core@shell NPs lies in the green region even at high pump power densities. The calculated colour coordinates for core@shell NPs at different pump power densities are found to be fixed at (0.29, 0.70). Further, on varying the temperature the colour coordinate value lies in the green region at (0.29, 0.70) {ESM Fig. 2 (b)}. Thus, it is obvious that the colour emitted by the developed core@shell NPs is not tuned on varying the pump power density and temperature.

The colour purity of the developed core@shell NPs can be calculated by using the following equation,

$$\text{Colour purity} = \frac{\sqrt{(X_s - X_i)^2 + (Y_s - Y_i)^2}}{\sqrt{(X_d - X_i)^2 + (Y_d - Y_i)^2}} x100\%$$

where, ($X_s$, $Y_s$) are the coordinates of a sample point, ($X_d$, $Y_d$) are the coordinate of the dominant wavelength and ($X_i$, $Y_i$) are the coordinates of illuminant point. The coordinate of the illuminant point is (0.3101, 0.3162). The colour purity of the prepared core and core shell NPs is found to be 92.02% and 95.30%, respectively.

The prepared core@shell NPs have also been utilized for security ink applications {Fig. 4 (d)}. The ink was prepared by dissolving 0.25 gm of the core@shell NPs in 5.0 ml acetone. The letters PHY were written on a white paper and they are not visible under normal day light illumination, but it could be seen in dark condition by illuminating with a 980 nm CW laser diode at 34.84 W/cm$^2$ of pump power density.

## 4. Conclusions

In conclusion, the developed multifunctional core@shell NPs with particle size ~50 nm have been successfully structurally and optically characterized. The representative EDS analysis confirms the presence of all the elements (Ho, Yb, Y, Mo) in the NPs, whereas silica layer is across the NPs. Due to presence of silica layer, the core@shell NPs show both the colloidal stability as well as high dispersibility in protic and aprotic polar solvents respectively. The core@shell NPs enhances the luminescence intensity than that of the core NPs due to reduction in the surface defects. A DLS and zeta potential measurement supports the good stability of the NPs in water. The difference in the UC emission intensity for the three kinds of solvents (Water, DMSO, methanol) arises due to different scattering behavior of the NPs. This is basically due to different colloidal stability of the suspensions in these solvents. Based on the experimental observations, it is believed that the developed core@shell NPs can be used for photonic, security ink and biological applications.

## Acknowledgements

Authors are grateful to Council of Scientific and Industrial Research (CSIR), New Delhi, India for financial assistance in the form of a research project {03(1354)/16/EMR-II}. One of the authors Manisha Mondal is also thankful to IIT (ISM), Dhanbad for providing the Junior Research Fellowship.

## Appendix A. Supplementary data

Supplementary data related to this article can be found at https://doi.org/10.1016/j.jallcom.2018.03.148.

## References


[1] X. Huang, Enhancement of near-infrared to near-infrared upconversion luminescence in sub-10-nm ultra-small $LaF_3:Yb^{3+}/Tm^{3+}$ nanoparticles through lanthanide doping, Opt. Lett. 40 (2015) 5231–5234.

[2] X. Yu, M. Xie, L. Chen, Y. Li, Q. Wang, Dopant-controlled synthesis of water-soluble hexagonal $NaYF_4$ nanorods with efficient upconversion fluorescence for multicolor bioimaging, Nano Res. 3 (2010) 51–60.

[3] L. Marciniak, K. Prorok, L. Francés-Soriano, J. Pérez-Prieto, A. Bednarkiewicz, A broadening temperature sensitivity range with a core–shell YbEr@YbNd double ratiometric optical nanothermometer, Nanoscale 8 (2016) 5037–5042.

[4] E.C. Ximendes, U. Rocha, C. Jacinto, K.U. Kumar, D. Bravo, F.J. López, E.M. Rodríguez, J.G. Solé, D. Jaque, Self-monitored photothermal nanoparticles based on core–shell engineering, Nanoscale 8 (2016) 3057–3066.

[5] Z. Zang, All optical switching in sagnac loop mirror containing an ytterbium-doped fiber and fiber Bragg grating, Appl. Optic. 52 (2013) 5701–5706.

[6] Z. Zang, Y. Zhang, Analysis of optical switching in a $Yb^{3+}$-doped fiber Bragg grating by using self modulation and cross phase modulation, Appl. Optic. 51 (2012) 3424–3430.

[7] Z. Zang, Y. Zhang, Low switching power (<45 mW) optical bistability based on optical nonlinearity of ytterbium-doped fiber with a fiber Bragg grating pair, J. Mod. Optic. 59 (2012) 161–165.

[8] M. Hegazy, P. Zhou, G. Wu, L. Wang, N. Rahoui, N. Taloub, X. Huang, Y. Huang, Construction of polymer coated core–shell magnetic mesoporous silica nanoparticles with triple responsive drug delivery, Polym. Chem. 8 (2017) 5852–5864.

[9] S. Hou, Y. Chi, Z. Zhao, Synthesis of core-shell structured magnetic nanoparticles with a carbide shell, IOP Conf. Ser.: Mater. Sci. Eng. 182 (2017), 012026 (1-5).

[10] Z. Wu, C. Guo, S. Liang, H. Zhang, L. Wang, H. Sun, A pluronic F127 coating strategy to produce stable up-conversion $NaYF_4$:Yb,Er(Tm) nanoparticles in culture media for bioimaging, J. Mater. Chem. 22 (2012) 18596–18602.

[11] M.S. Moorthy, B. Subramanian, M. Panchanathan, S. Mondal, H. Kim, K.D. Lee, J. Oh, Fucoidan-coated core–shell magnetic mesoporous silica nanoparticles for chemotherapy and magnetic hyperthermia-based thermal therapy applications, New J. Chem. 41 (2017) 15334–15346.

[12] T. Zhao, N. Nguyen, Y. Xie, X. Sun, Q. Li, X. Li, Inorganic nanocrystals functionalized mesoporous silica nanoparticles: fabrication and enhanced bioapplications, Front. Chem. 5 (2017). Article 118 (1–8).

[13] S. Shikha, T. Salafi, J. Cheng, Y. Zhang, Versatile design and synthesis of nanobarcodes, Chem. Soc. Rev. 46 (2017) 7054–7093.

[14] Q. Shao, Z. Yang, G. Zhang, Y. Hu, Y. Dong, J. Jiang, Multifunctional lanthanide-doped core/shell nanoparticles: integration of upconversion luminescence, temperature sensing, and photothermal conversion properties, ACS Omega 3 (2018) 188–197.

[15] Z. Li, J.K. Muiruri, W. Thitsartarn, X. Zhang, B.H. Tan, C. He, Biodegradable silica rubber core-shell nanoparticles and their stereocomplex for efficient PLA toughening, Compos. Sci. Technol. 159 (2018) 11–17.

[16] H. Wang, R. Han, L. Yang, J. Shi, Z. Liu, Y. Hu, Y. Wang, S. Liu, Y. Gan, Design and synthesis of core–shell–shell upconversion nanoparticles for nir-induced drug release, photodynamic therapy, and cell imaging, ACS Appl. Mater. Interfaces 8 (2016) 4416–4423.

[17] P.L. Abbaraju, Y. Yang, M. Yu, J. Fu, C. Xu, C. Yu, Core–Shell-structured dendritic mesoporous silica nanoparticles for combined photodynamic therapy and antibody delivery, Chem. Asian J. 12 (2017) 1465–1469.

[18] C. Kuiyong, H. Xiaobin, W. Hao, T. Xiaozhen, Fabrication of core/shell structured $NaYF_4:Yb^{3+}$, $Er^{3+}$/polyphosphazene upconversion nanophosphors functionalized with abundant active amino groups, Mater. Lett. 101 (2013) 54–56.

[19] R. Rajendran, L.K. Shrestha, K. Minami, M. Subramanian, R. Jayavel, K. Ariga, Dimensionally integrated nanoarchitectonics for a novel composite from 0D, 1D, and 2D nanomaterials: RGO/CNT/$CeO_2$ ternary nanocomposites with electrochemical performance, J. Mater. Chem. A 2 (2014) 18480–18487.

[20] A.K. Parchur, A.I. Prasad, A.A. Ansari, S.B. Rai, R.S. Ningthoujam, Luminescence properties of $Tb^{3+}$-doped $CaMoO_4$ nanoparticles: annealing effect, polar medium dispersible, polymer film and core–shell formation, Dalton Trans. 41 (2012) 11032–11045.

[21] J. Chen, Y. Sheng, Y. Song, M. Chang, X. Zhang, L. Cui, D. Meng, H. Zhu, Z. Shi, H. Zou, Multimorphology mesoporous silica nanoparticles for dye adsorption and multicolor luminescence applications, ACS Sustain. Chem. Eng. 6 (2018) 3533–3545.

[22] X.J. Wang, Y.R. Qu, Y.L. Zhao, H.B. Chu, Effect of the composition of lanthanide complexes on their luminescence enhancement by Ag@SiO2 core-shell nanoparticles, Nanomaterials 8 (2018) 98 (1-13).

[23] Y. Cheng, K. Sun, Upconversion photoluminescence of core-shell structured $SiO_2$@$YVO_4:Yb^{3+}$, $Er^{3+}$, $Eu^{3+}$ nanospheres, Appl. Optic. 56 (2017) 4905–4910.

[24] K. Matsumoto, M. Hagiwara, S. Fujihara, Fabrication of luminescent antireflective coatings with $CaMoO_4:Eu^{3+}$/Ag composite structure, Coatings 7 (2017) 74 (1-10).

[25] M. Mondal, V.K. Rai, C. Srivastava, Influence of silica surface coating on optical properties of $Er^{3+}$-$Yb^{3+}$:$YMoO_4$ upconverting nanoparticles, Chem. Eng. J. 327 (2017) 838–847.

[26] E. Banks, M. Nemiroff, Scheelite-type rare earth molybdates (V) and -(VI). $Eu_xMoO_4$ and $LnMoO_4$, Inorg. Chem. 13 (1974) 2715–2718.

[27] R.D. Shannon, Revised effective ionic radii and systematic studies of interatomic distances in halides and chalcogenides, Acta Crystallogr. 32 (1976) 751–767.

[28] A. Pandey, V.K. Rai, R. dey, K. Kumar, Enriched green upconversion emission in combustion synthesized $Y_2O_3$: $Ho^{3+}$–$Yb^{3+}$ phosphor, Mater. Chem. Phys. 139 (2013) 483–488.

[29] M. Mondal, V.K. Rai, C. Srivastava, S. Sarkar, R. Akash, Enhanced frequency upconversion in $Ho^{3+}/Yb^{3+}/Li^{+}$:$YMoO_4$ nanophosphors for photonic and security ink applications, J. Appl. Phys. 120 (2016), 233101 (1-11).

[30] H.L. Ding, Y.X. Zhang, S. Wang, M.J. Xu, S.C. Xu, G.H. Li, $Fe_3O_4$@$SiO_2$ core/shell nanoparticles: the silica coating regulations with a single core for different core sizes and shell thicknesses, Chem. Mater. 24 (2012) 4572–4580.

[31] K.M. Lin, C.C. Lin, Y.Y. Li, Synthesis silica sphere and core@shell $Gd_2O_3:Eu^{3+}$@$SiO_2$ phosphor nanoparticles by sol-gel method, Nanotechnology 1 (2006) 745–748.

[32] M. Secu, M. Cernea, C.E. Secu, B.S. Vasile, Structural and optical properties of fluorescent BaFBr-$Eu^{2+}$@$SiO_2$ core/shell phosphor heterostructure, Mater. Chem. Phys. 151 (2015) 81–86.

[33] A.A. Ansari, R. Yadav, S.B. Rai, Enhanced luminescence efficiency of aqueous dispersible $NaYF_4$:Yb/Er nanoparticles and the effect of surface coating, RSC Adv. 6 (2016) 22074–22084.

[34] A. Patterson, The scherrer formula for X-ray particle size determination, Phys. Rev. 56 (1939) 978–982.

[35] A.K. Singh (Ed.), Advanced X-ray Techniques in Research and Industries, Ios Pr Inc, 2005, ISBN 1586035371.

[36] S. Som, S.K. Sharma, T. Shripathi, Influences of doping and annealing on the structural and photoluminescence properties of $Y_2O_3$ nanophosphors, J. Fluoresc. 23 (2013) 439–450.

[37] P. Singh, A. Kumar, A. Kaushal, D. Kaur, A. Pandey, R.N. Goyal, In situ high temperature XRD studies of ZnO nanopowder prepared via cost effective ultrasonic mist chemical vapour deposition, Bull. Mater. Sci. 31 (2008) 573–577.

[38] V.S. Marques, L.S. Cavalcante, J.C. Sczancoski, A.F.P. Alcantara, M.O. Orlandi, E. Moraes, E. Longo, J.A. Varela, M.S. Li, M.R.M.C. Santos, Effect of different solvent ratios (Water/Ethylene Glycol) on the growth process of $CaMoO_4$ crystals and their optical properties, Cryst. Growth Des. 10 (2010) 4752–4768.

[39] A.A. Ansari, M. Alam, A.K. Prachur, Nd-doped calcium molybdate core and particles: synthesis, optical and photoluminescence studies, Appl. Phys. A 116 (2014) 1719–1728.

[40] A.A. Ansari, M. Alam, J.P. Labis, S.A. Alrokayan, G. Shafi, T.N. Hasan, N.A. Syed, A.A. Alshatwi, Luminescent mesoporous $LaVO_4:Eu^{3+}$ core@shell nanoparticles: synthesis, characterization, biocompatibility and their cytotoxicity, J. Mater. Chem. 21 (2011) 19310–19316.

[41] C. Wang, L. Cheng, Z. Liu, Upconversion nanoparticles for photodynamic therapy and other cancer therapeutics, Theranostics 3 (2013) 317–330.

[42] S. Som, S.K. Sharma, $Eu^{3+}/Tb^{3+}$-codoped $Y_2O_3$ nanophosphors: rietveld refinement, bandgap and photoluminescence optimization, J. Phys. D Appl. Phys. 45 (2012) 415102 (1-11).

[43] I. Hartenbach, S. Strobel, T. Schleid, B. Sarkar, W. Kaim, P. Nockemann, K. Binnemans, P.K. Dorhout, Synthesis, structure, and spectroscopic properties of the New lanthanum(III) fluoride oxomolybdate(VI) $La_3FMo_4O_{16}$, Eur. J. Inorg. Chem. (2010) 1626–1632.

[44] A. Pandey, V.K. Rai, Improved luminescence and temperature sensing performance of $Ho^{3+}$–$Yb^{3+}$–$Zn^{2+}$:$Y_2O_3$ phosphor, Dalton Trans. 42 (2013) 11005–11011.

[45] A.K. Soni, V.K. Rai, $BaZnLa_2O_5:Ho^{3+}$-$Yb^{3+}$ phosphor for display and security ink application, J. Opt. Soc. Am. B 31 (2014) 1814–1821.

[46] O.A. Sanchuk, J.J. Carvayal, C. Cascales, M. Aguilo, F. Diaz, Benefits of silica core–shell structures on the temperature sensing properties of Er,Yb:$GdVO_4$ up-conversion nanoparticles, ACS Appl. Mater. Interfaces 8 (2016) 7266–7273.

[47] F. Zhang, R.C. Che, X.M. Li, C. Yao, J.P. Yang, D.K. Shen, P. Hu, W. Li, D.Y. Zhao, Direct imaging the upconversion nanocrystal core/shell structure at the subnanometer level: shell thickness dependence in upconverting optical properties, Nano Lett 12 (2012) 2852–2858.

[48] F. Vetrone, R. Naccache, V. Mahalingam, C.G. Morgan, J.A. Capobianco, The active-core/active-shell approach: a strategy to enhance the upconversion luminescence in lanthanide-doped nanoparticles, Adv. Funct. Mater. 19 (2009) 2924–2929.

[49] N.J.J. Johnson, F.C.J.M. Van Veggel, Sodium lanthanide fluoride core@shell nanocrystals: a general perspective on epitaxial shell growth, Nano Res. 6 (2013) 547–561.

[50] H. Lu, H. Hao, G. Shi, Y. Gao, R. Wang, Y. Song, Y. Wang, X. Zhang, Optical temperature sensing in β-$NaLuF_4:Yb^{3+}/Er^{3+}/Tm^{3+}$ based on thermal, quasi-thermal and non-thermal coupling levels, RSC Adv. 6 (2016) 55307–55311.

[51] R. Dey, V.K. Rai, $Yb^{3+}$ sensitized $Er^{3+}$ doped $La_2O_3$ phosphor in temperature sensors and display devices, Dalton Trans. 43 (2014) 111–118.

[52] R.C. Hilborn, Einstein coefficients, cross sections, f values, dipole moments and all that, Am. J. Phys. 50 (1982) 982–986.

[53] S.J. Strickler, R.A. Berg, Relationship between absorption intensity and

fluorescence lifetime of molecules, J. Chem. Phys. 37 (1962) 814–822.
[54] V.A. Durov, A.P. Moscalets, Deformation C–S and S=O bond polarizations in dimethyl sulfoxide, Russ. J. Phys. Chem. 85 (2011) 338–340.
[55] A.D. Vyas, V.A. Rana, D.H. Gadani, Dielectric properties of mixtures of some rigid polar molecules with some primary alcohols, Indian J. Pure Appl. Phys. 49 (2011) 277–283.
[56] J.K. Gregory, D.C. Clary, K. Liu, M.G. Brown, R.J. Saykally, The water dipolar moment in water clusters, Science 275 (1997) 814–817.
[57] S.H. Sohn, J.H. Lee, S.M. Lee, Effects of the surface coating of $BaMgAl_{10}O_{17}:Eu^{2+}$ phosphor with $SiO_2$ nano-particles, J. Lumin. 129 (2009) 478–481.